1 Constant density

We consider the vertical cross-section in a wind-driven lake of constant depth H and horizontal extent L. The kinematic viscosity ν is constant. A no-slip condition is applied on the bottom boundary ($u = w = 0$). The top boundary is a "rigid lid" and the effect of the wind is modelled as an imposed velocity gradient i.e. $w = 0$ and $\partial_z u = \tau$. The left and right wall use "slip conditions" i.e. ($u = 0$, $\partial_x w = 0$). The assumption of a rigid lid rather than a free surface is justified when the speed of the gravity waves $\sqrt{g\,H}$ is large compared to the physical velocities (i.e. the Froude number is small) or equivalently, when the slope of the free surface is small. Using dimensional arguments, this slope can be estimated as

$$\frac{\nu\,\tau}{g\,H}$$

The independent dimensionless numbers controlling the problem then are:

- the aspect ratio $a = L/H$,
- a Reynolds number $\mathrm{Re} = H\,\tau^2/\nu$,
- the free-surface slope $\alpha = \nu\,\tau/g\,H$.

In the following, we consider only dimensionless quantities where H has been taken as length scale and $1/\tau$ as time scale.

An analytical solution for this problem can be obtained in the limit of large a and assuming a parallel flow. A parabolic velocity profile of the form

$$u(z) = A\,z^2 + B\,z + C$$

is sought. An additional constraint must thus be added to the two boundary conditions above in order to close the system. This is provided by observing that volume conservation requires that the depth-averaged velocity be zero. One then easily gets

$$u(z) = \frac{z}{4}\,(3\,z - 2).$$

This can also be used to refine the free-surface slope estimate using the equilibrium relationship

$$\partial^2_{z^2} u = \frac{\alpha'}{\alpha},$$

where we assume hydrostatic balance. For the parabolic velocity profile, this gives

$$\alpha' = \frac{3}{2}\alpha \tag{1}$$

In the case of a finite aspect ratio a, we expect this solution to be valid only in the center of the lake, where the hypothesis of parallel flow should be verified. The "upwelling" and "downwelling" zones close to the side walls will of course not be described by this solution.

To verify this hypothesis, we used Gerris to solve the incompressible Navier-Stokes equations in a rectangular domain with the boundary conditions given above. For low Reynolds numbers, a stationary solution to this variant of the "lid-driven cavity" problem can be readily obtained. Figure 1 illustrates the stationary solution obtained numerically for $a = 4$, $\mathrm{Re} = 1$, discretised with 32 points both horizontally and vertically.

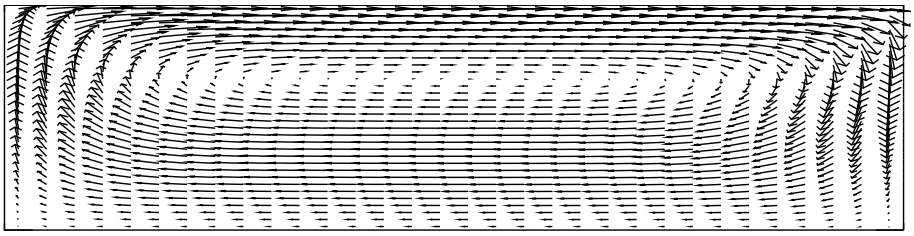

Figure 1. Velocity field for the wind-driven lake. $a = 4$, $\mathrm{Re} = 1$.

Figure 2 illlustrates the velocity profile obtained numerically in the center of the lake together with the analytical solution, while Figure 3 illustrates the superposition of pressure values in the domain together with the equilibrium solution (1).

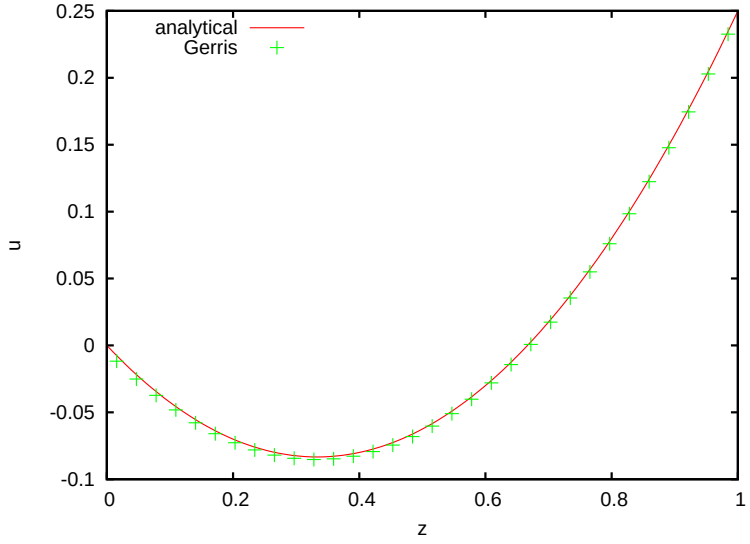

Figure 2. Velocity profile in the center of the lake. $a = 4$, $\mathrm{Re} = 1$.

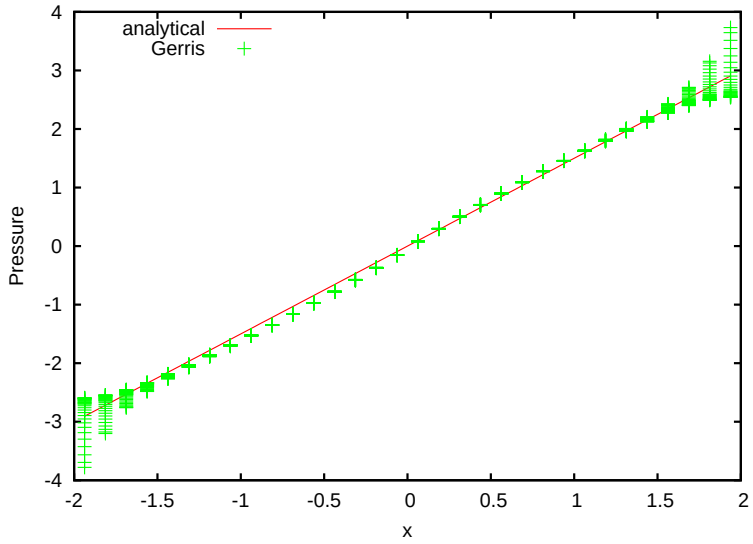

Figure 3. Values of pressure together with the analytical solution (equation (1)). $a = 4$, $\mathrm{Re} = 1$.

It is clear that the analytical solution is a good approximation even for this low aspect ratio. An indication of the lower limit of validity of the solution is given by Figure 4 where the aspect ratio has been varied from 1 to 8 while keeping all the other parameters constant.

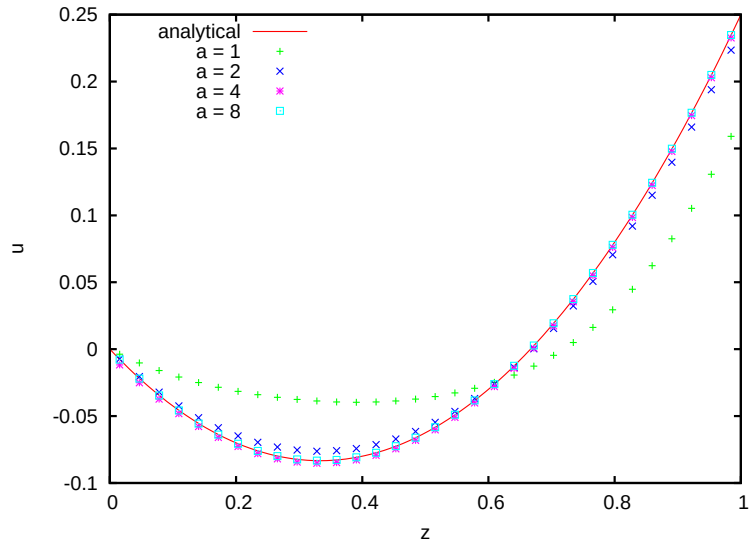

Figure 4. Convergence of the velocity profiles in the center of the lake as a function of the aspect ratio. $\mathrm{Re} = 1$.

What is the effect of the Reynolds number? Figure 5 illustrates the stationary velocity field obtained for $a = 4$ and $\mathrm{Re} = 400$. There is a clear lateral asymmetry with a strong localised downwelling and a broad and weak upwelling compared to Figure 1. Note that this is similar to what is classically observed for the lid-driven cavity problem at comparable Reynolds numbers (with aspect ratios close to unity).

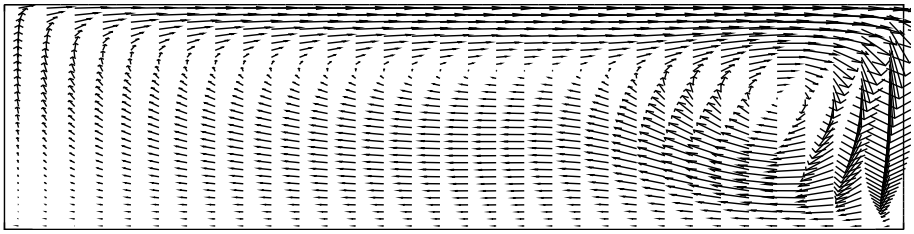

Figure 5. Velocity field for the wind-driven lake. $a = 4$, $\mathrm{Re} = 400$.

This asymmetry also affects the assumption of parallel flow in the center of the lake and the analytical solution is only recovered for significantly larger aspect ratios (Figure 6). The same holds for the pressure profiles (Figure 7).

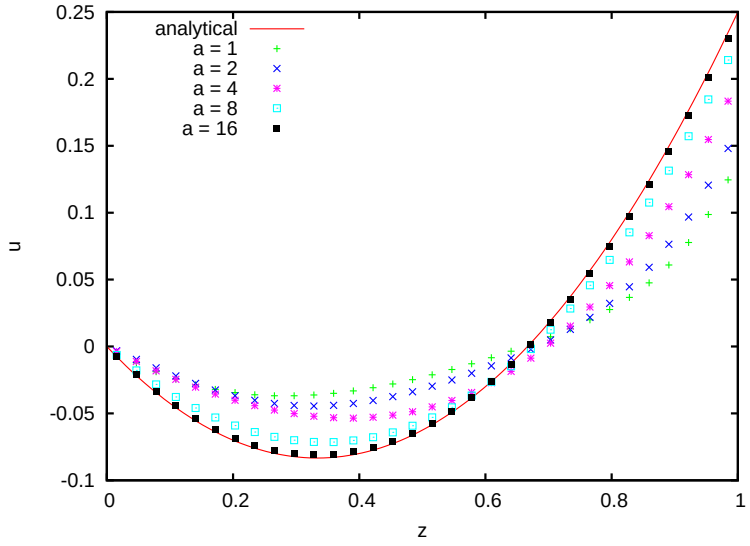

Figure 6. Convergence of the velocity profiles in the center of the lake as a function of the aspect ratio. $\mathrm{Re} = 400$.

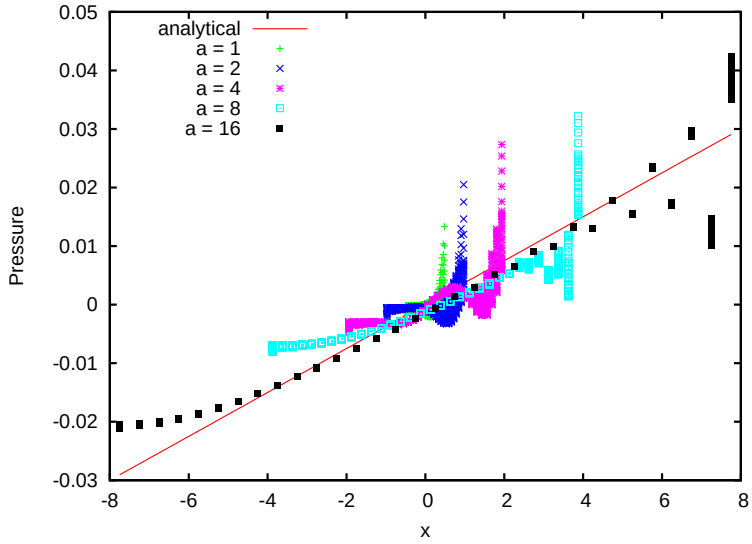

Figure 7. Convergence of the pressure profiles as a function of the aspect ratio. Re = 400.

The lateral upwelling and downwelling are important features of the wind-driven circulation and it is useful to caracterise their lateral extent. This can be done using several methods. Given the good predictions in the center of the lake obtained with the simple parallel flow analytical model, one way to caracterise the lateral currents is to measure the departure from the parallel flow analytical solution. We define the depth-averaged root-mean-square (RMS) error norm as

$$e_{\mathrm{RMS}}(x) = \sqrt{\int \left(u(x,z) - u_{\mathrm{analytical}}(z)\right)^2 dz}.$$

Figure 8 illustrate this error distribution for Re = 1 and Re = 400 for different aspect ratios. Consistently with Figures 4 and 6, the error in Figure 8.a is negligible in the center of the lake for aspect ratios larger than 4, while the error in Figure 8.b is still significant for $a = 16$. The asymmetry of the flow for Re = 400 is also evident.

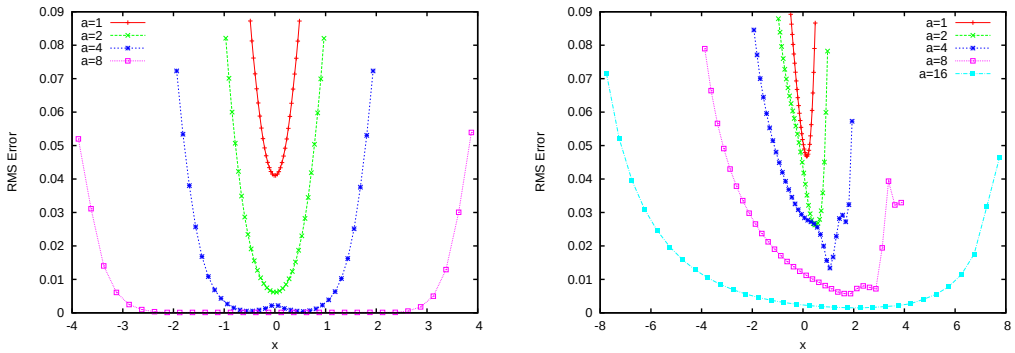

Figure 8. Error distribution $e_{\mathrm{RMS}}(x)$ for (a) Re = 1 (b) Re = 400.

It is clear that as the central part of the lake converges toward the parallel flow solution (with increasing aspect ratio), the solutions for the lateral upwelling and downwelling should

become independent from each other and thus from the aspect ratio. This can be verified by changing the reference of the horizontal axis of Figure 8 to make it coincide with the lateral boundaries. This is what is done in Figure 9.

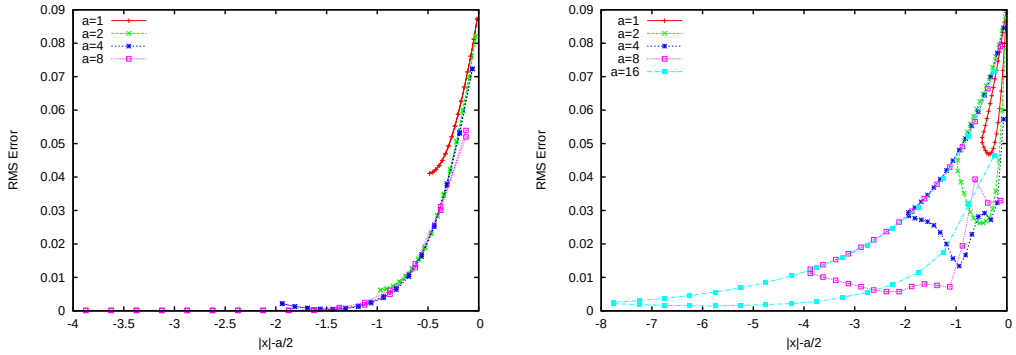

Figure 9. Error distribution $e_{\mathrm{RMS}}(x)$ for (a) $\mathrm{Re}=1$ (b) $\mathrm{Re}=400$.

An alternative description of the lateral upwelling and downwelling is given by looking at the depth-averaged vertical velocity profile (Figures 10 and 11).

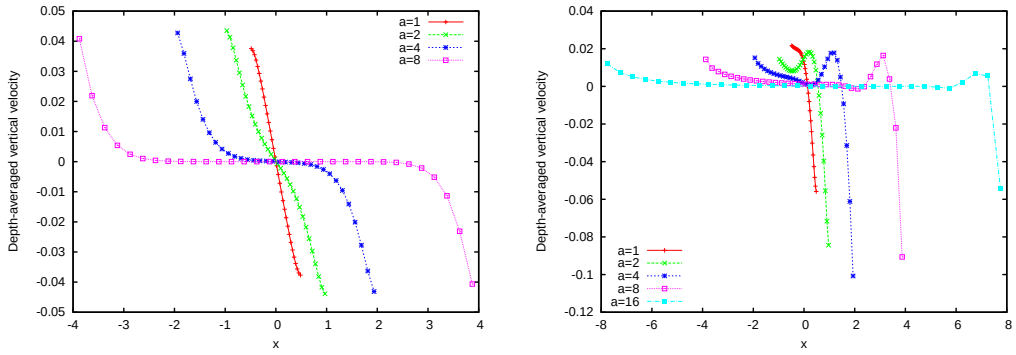

Figure 10. Depth-averaged vertical velocity $\bar{w}(x)$ for (a) $\mathrm{Re}=1$ (b) $\mathrm{Re}=400$.

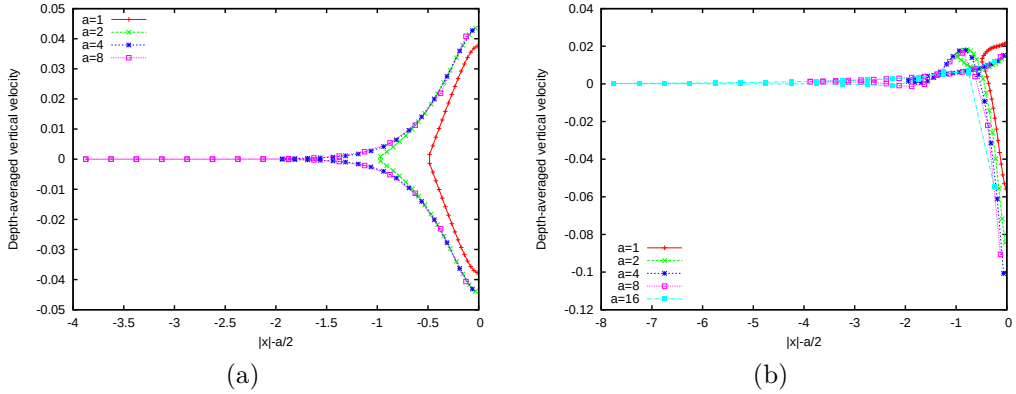

Figure 11. Depth-averaged vertical velocity $\bar{w}(x)$ for (a) $\mathrm{Re}=1$ (b) $\mathrm{Re}=400$.

1.1 Parabolic bathymetry

We now consider a lake with variable depth

$$H(x) = 1 - 4\frac{x^2}{a^2}$$

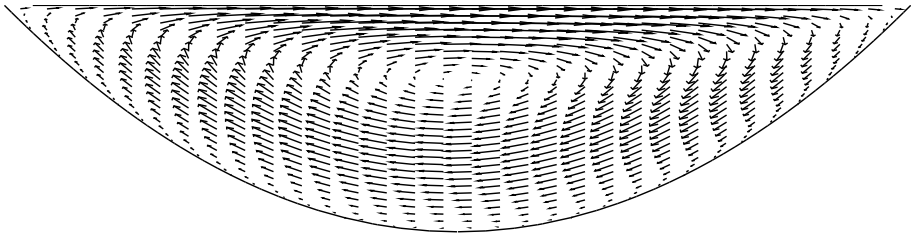

Figure 12. Velocity field for the wind-driven lake. $a = 4$, $\mathrm{Re} = 1$.

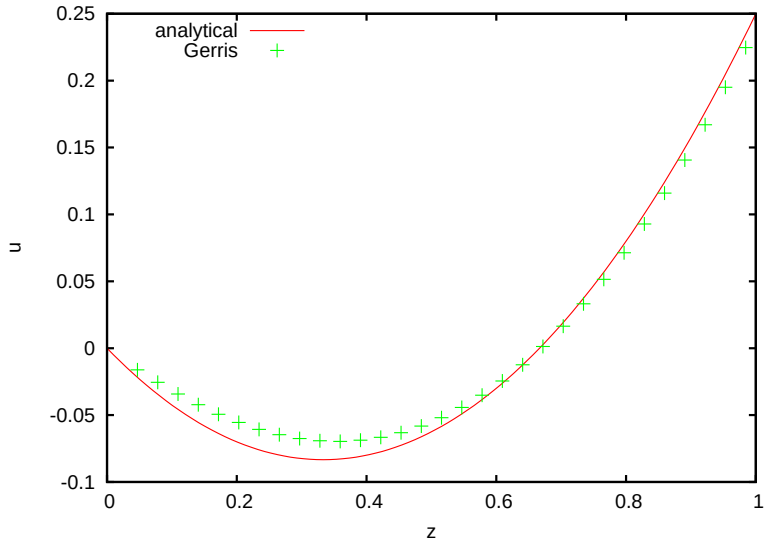

Figure 13. Velocity profile in the center of the lake. $a = 4$, $\mathrm{Re} = 1$.

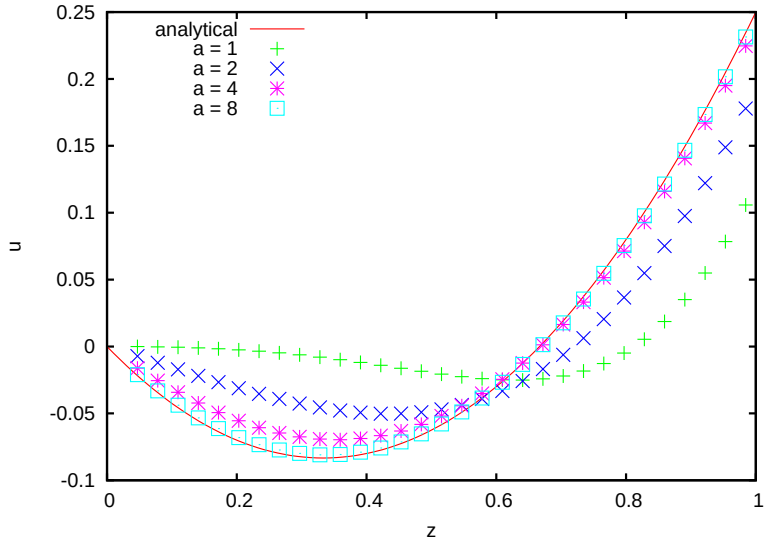

Figure 14. Convergence of the velocity profiles in the center of the lake as a function of the aspect ratio. $\mathrm{Re} = 1$.

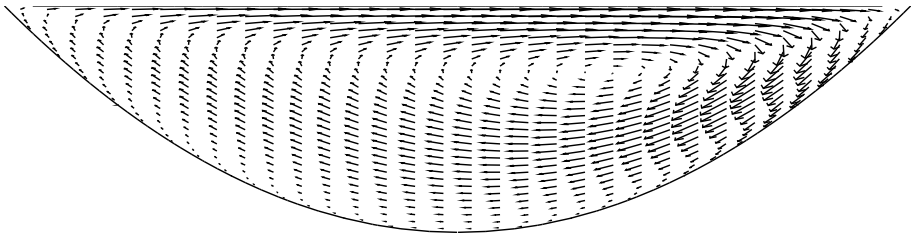

Figure 15. Velocity field for the wind-driven lake. $a = 4$, $\mathrm{Re} = 400$.

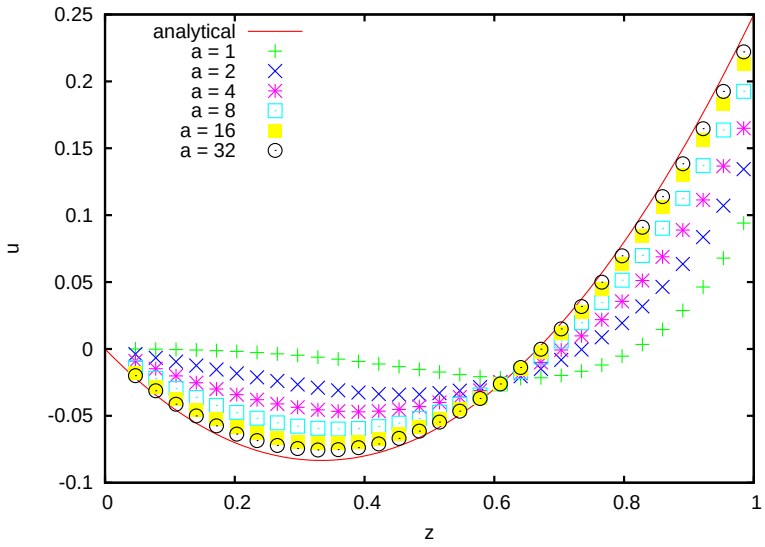

Figure 16. Convergence of the velocity profiles in the center of the lake as a function of the aspect ratio. $\mathrm{Re} = 400$.

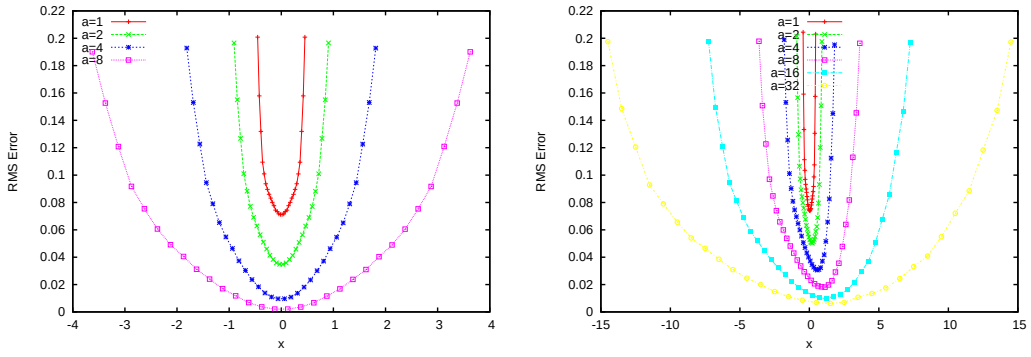

Figure 17. Error distribution $e_{\mathrm{RMS}}(x)$ for (a) $\mathrm{Re} = 1$ (b) $\mathrm{Re} = 400$.

In contrast to the constant-depth case, we expect the boundary currents to scale like the bathymetry so that the relevant variable now is x/a. This scaling is confirmed by the convergence observed for large aspect ratios in Figure 18.

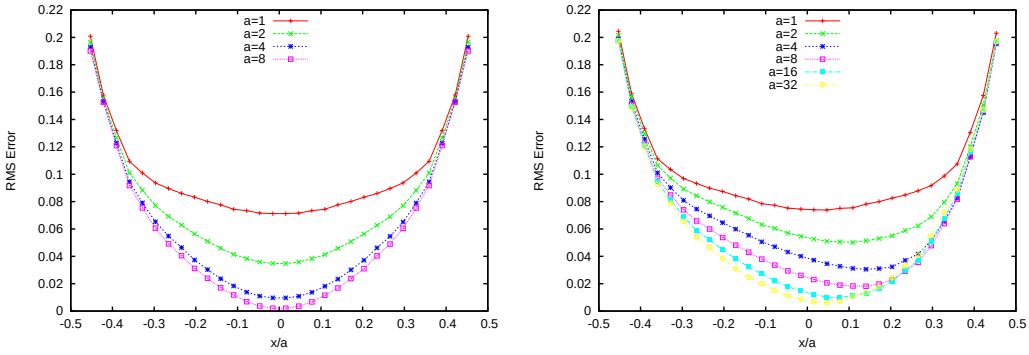

(a) (b)

Figure 18. Error distribution $e_{\mathrm{RMS}}(x)$ for (a) $\mathrm{Re}=1$ (b) $\mathrm{Re}=400$.

The magnitude of the vertical velocity is expected to scale like $1/a$ (Figure 20).

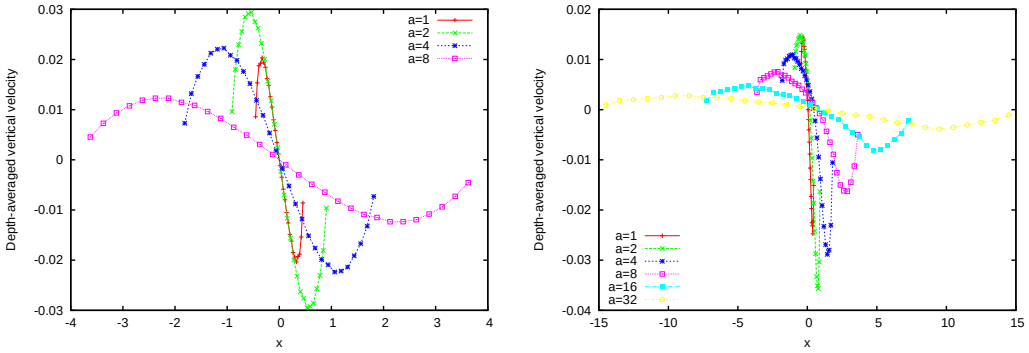

(a) (b)

Figure 19. Depth-averaged vertical velocity $\bar{w}(x)$ for (a) $\mathrm{Re}=1$ (b) $\mathrm{Re}=400$.

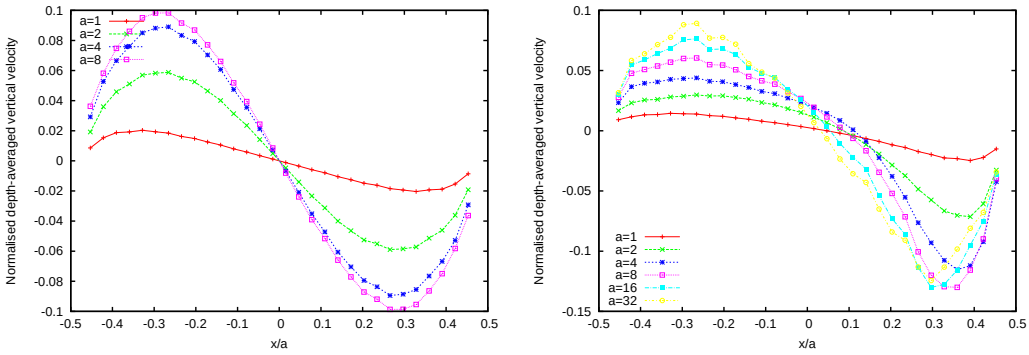

(a) (b)

Figure 20. Normalised depth-averaged vertical velocity $a\,\bar{w}(x)$ as a function of normalised abscissa x/a for (a) $\mathrm{Re}=1$ (b) $\mathrm{Re}=400$.

1.1.1 Three-dimensional paraboloidal bathymetry

The depth is described by

$$H(x,y)=1-4\,\frac{(x^2+y^2)}{a^2}$$

Each dimension is discretised with 32 grid points. The overall stationary circulation is depicted in Figure 21. The vertical profile of horizontal velocity at the center of the lake is given in Figure 22 together with the analytical model. While the 3D solution does verify the top and bottom boundary conditions, it does not verify the additional constraint of volume conservation in a vertical slice (i.e. nullity of the depth-averaged horizontal velocity). This is not surprising since the flow structure is clearly three-dimensional and horizontal divergence also needs to be taken into account when looking at volume conservation.

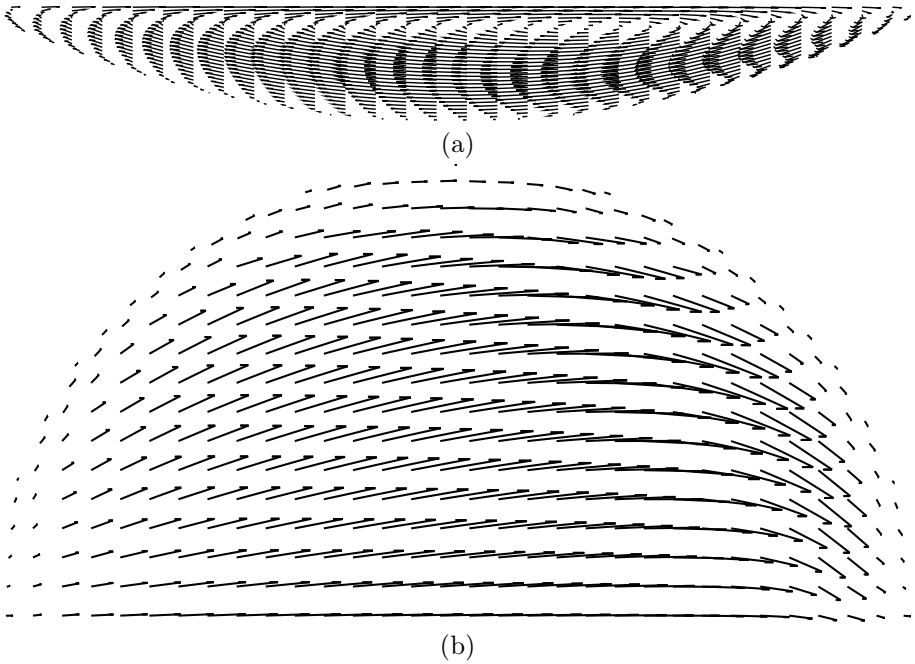

Figure 21. Velocity field for the three-dimensional wind-driven lake. $a = 8$, $\mathrm{Re} = 400$. (a) cross-section at $y = 0$. (b) cross-section at $z = 1$.

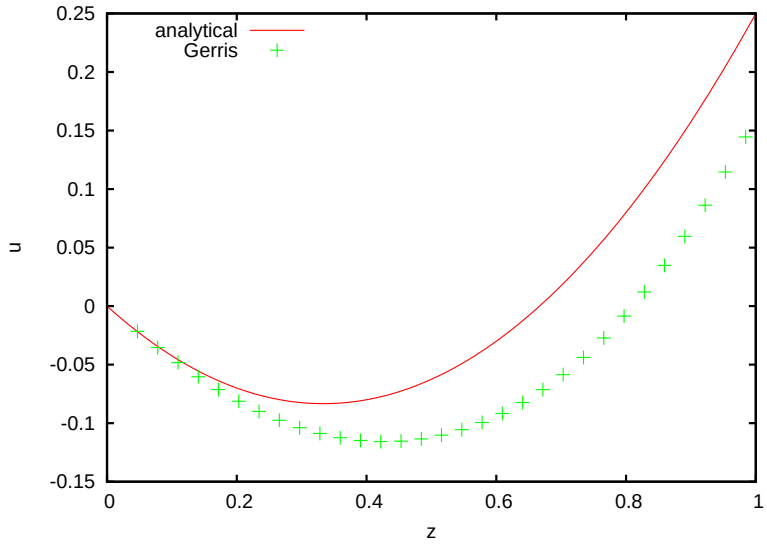

Figure 22. Vertical profile in the center of the lake. $a = 8$, $\mathrm{Re} = 400$.

2 Stratified lake

We now consider the case of a stratified lake. To model the stable thermal stratification often observed in lakes, we assume a vertical density profile of the form

$$\rho(z) = \rho_0 - H_{\text{eaviside}}(z - H + H_{\text{thermocline}})\,\Delta\rho.$$

If $\Delta\rho/\rho_0$ is small compared to one, we can use a Boussinesq approximation and this results in an additional source term $-\,g'\,H_{\text{eaviside}}(z\,-\,H\,+\,H_{\text{thermocline}})$ for the vertical component of velocity, with g' the reduced gravity

$$g' = \frac{\Delta\rho}{\rho_0}\,g.$$

Through dimensional arguments one can find that the equilibrium slope α_t of the thermocline should verify the relation

$$g'\,\alpha_t \;\propto\; \nu\,\tau,$$

for vanishing α_t.

We then need to consider two additional independent dimensionless parameters

- $b = 1 - H_{\text{thermocline}}/H$, set to 3/4 in what follows,
- and the thermocline slope

$$\alpha_t = \frac{\nu\,\tau}{g'\,H}$$

If we again assume parallel flow, an analytical solution can be sought for the horizontal velocity profile in a vertical cross-section, of the form

$$\begin{aligned} u(z) &= A_1\,z^2 + B_1\,z + C_1 \quad \text{for } z > b,\\ u(z) &= A_2\,z^2 + B_2\,z + C_2 \quad \text{for } z \leqslant b, \end{aligned}$$

with the boundary conditions

$$\begin{aligned} \partial_z u = 1 \quad & \text{at } z = 1,\\ u = 0 \quad & \text{at } z = 0,\\ u|_{z>b} = u|_{z<b} \quad & \text{at } z = b,\\ \partial_z u|_{z>b} = \partial_z u|_{z<b} \quad & \text{at } z = b, \end{aligned}$$

and the volume conservation conditions

$$\begin{aligned} \int_b^1 A_1\,z^2 + B_1\,z + C_1\,dz \;&= 0,\\ \int_0^b A_2\,z^2 + B_2\,z + C_2\,dz \;&= 0. \end{aligned}$$

Developing gives

$$\begin{aligned} 2\,A_1 + B_1 &= 1\\ A_1\,b^2 + B_1\,b + C_1 &= A_2\,b^2 + B_2\,b\\ 2\,A_1\,b + B_1 &= 2\,A_2\,b + B_2\\ A_1\,(1-b^3)/3 + B_1\,(1-b^2)/2 + C_1\,(1-b) &= 0\\ A_2\,b^3/3 + B_2\,b^2/2 &= 0 \end{aligned}$$

For $b = 3/4$, this readily gives

$$u(z) = \frac{30\,z^2 - 47\,z + 18}{13} \quad \text{for } z > 3/4,$$
$$u(z) = \frac{-2\,z^2 + z}{13} \quad \text{for } z \leqslant 3/4.$$

This can be used to refine the estimates of the thermocline and surface slopes. Assuming hydrostatic balance, the horizontal pressure gradient is given by

$$\partial_x p = g\,\alpha' \quad \text{for } z > 3/4 + \alpha_t'\,x,$$
$$\partial_x p = g\,\alpha' + g'\,\alpha_t' \quad \text{for } z \leqslant 3/4 + \alpha_t'\,x.$$

Balancing the horizontal pressure gradients and viscous stress then gives

$$\alpha' = \frac{60}{13}\,\alpha \tag{2}$$
$$\alpha_t' = -\frac{64}{13}\,\alpha_t \tag{3}$$

The interface between the two layers is tracked numerically using a Volume-Of-Fluid (VOF) scheme which is non-diffusive. Figure 23 illustrates the stationary velocity field as well as the interface between the two layers.

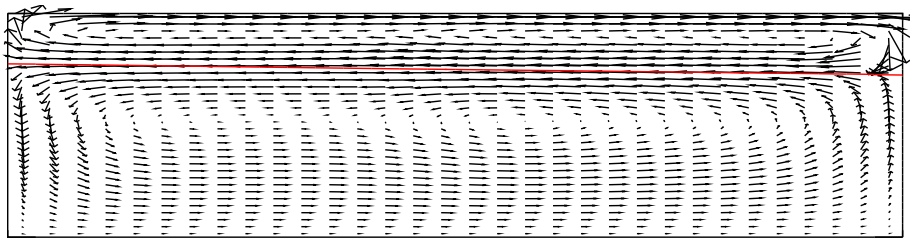

Figure 23. Velocity field for the wind-driven lake. $a = 4$, $\mathrm{Re} = 400$, $\alpha_t = 1/400$.

Figure 25 illlustrates the convergence of the velocity profile obtained numerically in the center of the lake toward the analytical solution.

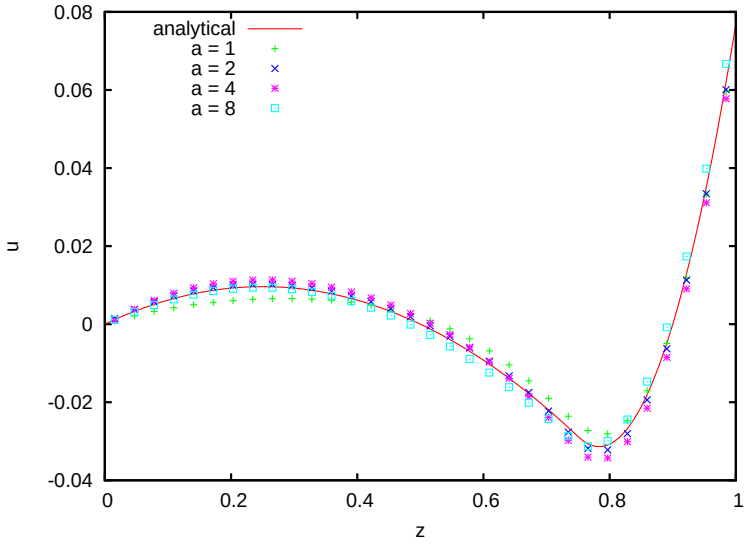

Figure 24. Convergence of the velocity profiles in the center of the lake as a function of the aspect ratio. $\mathrm{Re} = 400$, $\alpha_t = 1/400$.

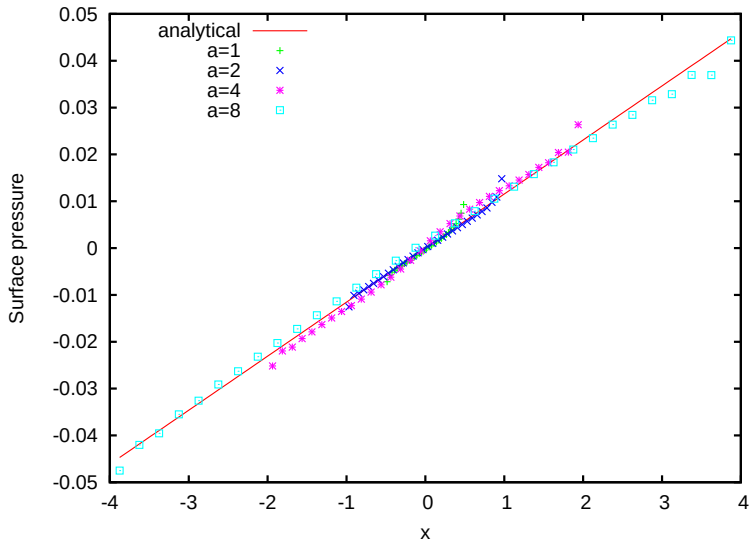

Figure 25. Convergence of the surface pressure profiles as a function of the aspect ratio. $\mathrm{Re} = 400$, $\alpha_t = 1/400$. The analytical solution is given by (2).

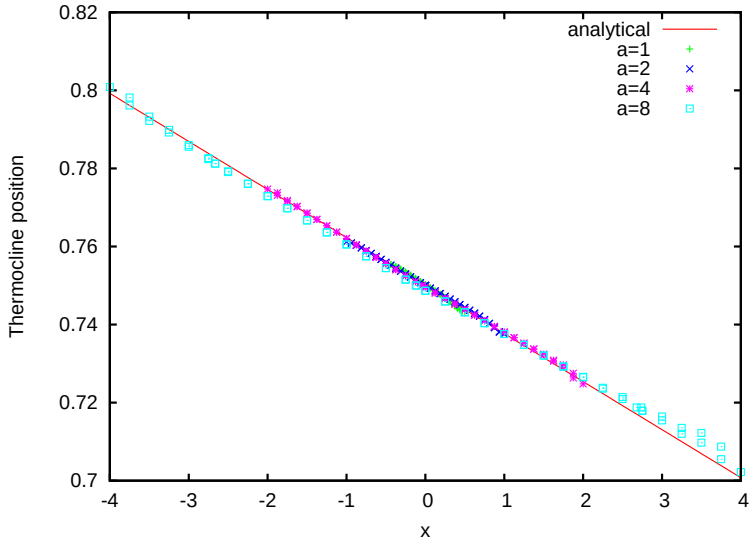

Figure 26. Convergence of the thermocline profiles as a function of the aspect ratio. $\mathrm{Re} = 400$, $\alpha_t = 1/400$. The analytical solution is given by (3).

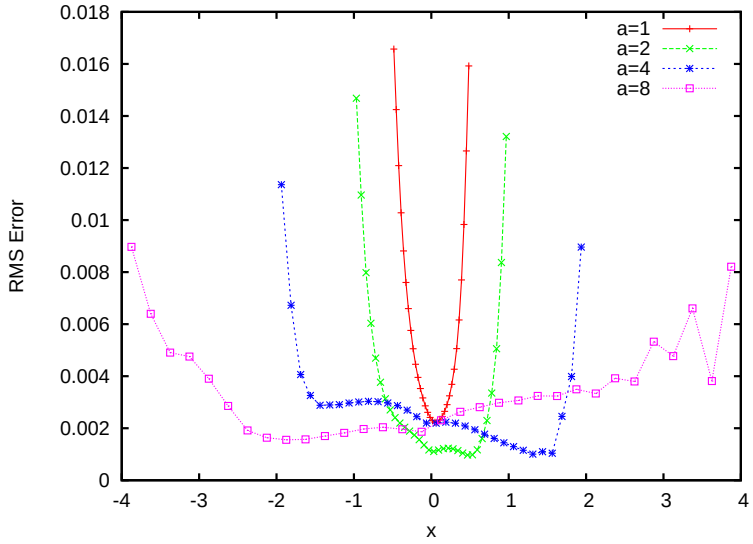

Figure 27. Error distribution $e_{\mathrm{RMS}}(x)$ for $\mathrm{Re} = 400$, $\alpha_t = 1/400$.

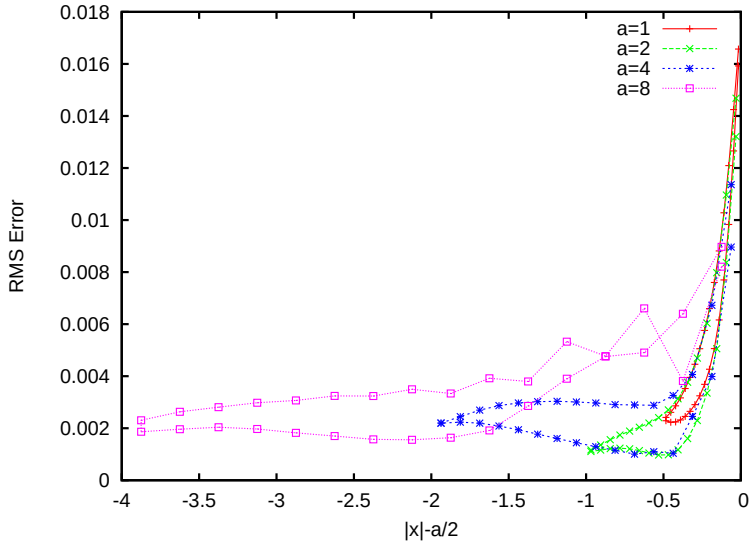

Figure 28. Error distribution $e_{\mathrm{RMS}}(x)$ for $\mathrm{Re} = 400$, $\alpha_t = 1/400$.